Mass Transfer in VOC Adsorption on Zeolite : Experimental and Theoretical Breakthrough Curves

Stephan Brosillon, Marie-Hélène Manero, Jean-Noel Foussard

Mass Transfer in VOC Adsorption on Zeolite: Experimental and Theoretical Breakthrough Curves

STEPHAN BROSILLON,*,†
MARIE-HELENE MANERO,‡ AND
JEAN-NOEL FOUSSARD†

Departement de Génie des Procédés Industriels, Laboratoire d'Ingenierie des Procédés de l'Environnement, Institut National des Sciences Appliquées, 135 Avenue de Rangueil, 31077 Toulouse Cedex 4, France, and Département de Génie Chimique, IUT Paul Sabatier, 18 ch de la Loge, BP4065 31029 Toulouse Cedex 4, France

From experimental results of adsorption of volatile organic compounds (VOCs) on zeolite, we propose simulations of the breakthrough curves based on the Linear Driving Force model. Experiments were run on fixed beds of hydrophobic commercial zeolites. Pollutants chosen are from several chemical classes with different polarities. A good agreement between experimental and numerical results is found when an adjustable value of the internal mass-transfer coefficient is used. A constant value of effective diffusivity is found independent of the nature and the amount of VOCs adsorbed. A relation linking intrapellet mass-transfer coefficient and equilibrium constant is proposed, including the average effective diffusivity, to make predictions of breakthrough curves for any kind of volatile organic pollutant in gaseous effluents.

Introduction

The removal of volatile organic compounds (VOCs) is of significant interest in air quality control. There are several chemical engineering processes that are commonly used in industry to deal with VOCs emissions. Incineration and biofiltration are classified as destructive techniques whereas condensation, scrubbing, and adsorption are considered as recuperative ones (1). In this paper, the focus is on the adsorption technique. Activated carbon is the most widely used material in industrial adsorption processes (2–6) but is not without problems. The use of zeolites may be an interesting alternative because these materials are stable at high temperature, keep good adsorption capacities under humid conditions, and are not flammable. Usual zeolite adsorption contactors are fixed packed beds or rotating wheel systems (7). To improve the industrial design of these adsorbers and to find the best operating conditions, the adsorption processes need to be modeled. To do this, gas–solid equilibrium experiments and adsorption kinetic experiments must be performed. Numerous models have been published in recent years to describe the phenomena of fixed bed adsorption. Detailed reviews have been proposed by Tien (5) and Ruthven (7). All these models are based on the following fundamental relations: transport phenomena equations (mass and heat), equilibrium isotherm equations, mass balance equations, boundary conditions, and initial conditions.

Many publications on modeling adsorption on activated carbon applications were reviewed during this work (8–10), but very few focused on the modeling of zeolite adsorption. Mass transfer can be described by the Linear Driving Force (LDF) model. This lumped-parameter model is based on the assumption that the uptake rate of adsorbate by a pellet is linearly proportional to a driving force. This driving force is defined as the difference between the surface concentration (pellet/gas interphase) and the average adsorbed-phase concentration (5). Recent studies (10–14) have given good results for modeling dynamic adsorption with this model. Moreover, its simplicity allows significant savings in computation time. The aim of this present study is to predict breakthrough curves of industrial solvent on a fixed bed of zeolite and to propose a correlation to predict the LDF mass-transfer coefficient. The accuracies of the predictions were assessed by comparing them with experimental breakthrough curves.

Theoretical Approach

The mathematical model of the isothermal, dynamic adsorption breakthrough process in a fixed bed is based on transient material balance, gas phase and intrapellet mass transfer, the adsorption equilibrium relationship, boundary conditions, and initial conditions. Both the adsorption equilibrium and kinetic aspect are taken into account. The adsorption equilibrium is described by the Langmuir equation (15). The mass-transfer rate is represented by the LDF model. The LDF model is a lumped-parameter model for particle adsorption. The estimation of the mass-transfer coefficient, k_p, is an important step in the resolution of the simulation problem. The assumptions made are common: the pressure drop is very low; the system is isothermal for low concentrations; the vapor is considered as an ideal gas; and the plug flow is assumed.

Mass Balance on Fixed Bed. If the flow rate is constant and the effect of axial dispersion is neglected, the mass balance on a portion of the bed is given by

{mass accumulation in the gas phase} +
{mass adsorbate in the solid phase} +
{mass flux} = 0

$$\epsilon \frac{dC}{dt} + \rho_1 \frac{dq}{dt} + u \frac{dC}{dz} = 0 \qquad (1)$$

Transfer in Gas Phase. The hypothesis of an external film around the particle is made:

$$\epsilon \frac{dC}{dt} + u \frac{dC}{dz} = -k_f S_p (C - C_s) \qquad (2)$$

The transfer in the gas phase depends on the flow condition around the pellet.

Intrapellet Mass Transfer. In this study, the LDF model was used to describe the intrapellet mass transfer:

$$\frac{dq}{dt} = k_p (q_s - q) \qquad (3)$$

The k_p parameter can be considered as an adjustable parameter (5, 10, 12). Thus, fitting simulation results and experimental data allows this parameter to be determined.

* Corresponding author phone: +33 561 55 97 56; fax: +33 561 55 97 60; e-mail: brosillo@insa-tlse.fr.
† Institut National des Sciences Appliquées.
‡ IUT Paul Sabatier.

Equilibrium Model. The adsorption capacities were deduced from equilibrium adsorption isotherms using the Langmuir isotherm model. Its general expression is as follows:

$$q = q_{max}\frac{bC}{1+bC} \tag{4}$$

The experimental isotherms we found were of type I in the IUPAC classification, which explains their good fit with the Langmuir model. This expression is thermodynamically consistent, as it respects Henry's law when $C \rightarrow 0$.

Boundary Conditions. (i) Equality of flux through the surface of the adsorbent leads to the following continuity equation:

$$k_f S_p(C - C_s) = \rho_1 k_p(q_s - q) \tag{5}$$

(ii) Concentration of the compound at the column inlet is the initial concentration, C_0:

$$C = C_0 \quad \text{for } z = 0 \text{ and } t > 0$$

Initial Conditions.

$$q = 0 \quad \text{for } z \geq 0 \text{ and } t = 0$$
$$C = C_0 \quad \text{for } z = 0 \text{ and } t = 0$$
$$C = 0 \quad \text{for } z > 0 \text{ and } t = 0$$

For the resolution, the mathematical model was changed into a dimensionless form. The numerical method was the Finite Difference Method. We used a forward finite difference explicit scheme. The resolution time ranged between 3 and 5 min.

Estimation of Mass-Transfer Coefficient, k_p. The mass-transfer coefficient (k_p) value was found by fitting the simulation breakthrough curves to experimental data. The LDF mass-transfer coefficient is related to mass-transfer resistance for a biporous spherical adsorbent as follows:

$$\frac{1}{k_p} = \frac{R_p}{3k_f} + \frac{R_p^2}{15\epsilon_p D_e}K + \frac{R_c^2}{15D_c} \tag{6}$$

with $K = (q\rho_p/C_e)$ equilibrium constant. Equation 6 is considered an extension of the Glueckauf approximation (17). If micropore resistance is neglected, eq 6 becomes

$$\frac{1}{k_p} = \frac{R_p}{3k_f} + \frac{R_p^2}{15\epsilon_p D_e}K \tag{7}$$

The effective diffusivity (D_e) was determined from eq 7 using the value of k_p. Knudsen diffusivity is given by the relation (18)

$$D_k = 9700 r_o\sqrt{\frac{T}{M}} \tag{8}$$

The effective diffusivity (D_e) is related to molecular, Knudsen, and surface diffusivities by means of eq 9 (12). With the values of D_e and D_k known, the surface diffusivity (D_s) was deduced from eq 9 with the assumption that pore tortuosity and surface tortuosity are equal (9):

$$\frac{1}{D_e} = \frac{\tau_p}{D_m} + \frac{1}{\dfrac{D_k}{\tau_p} + \dfrac{1-\epsilon_p}{\epsilon_p}\dfrac{D_s}{\tau_s}K} \tag{9}$$

Experimental Studies

Adsorbent. The adsorbent used is a silicalite, a commercial zeolite that has the MFI structure (17). A high Si/Al ratio

TABLE 1. Adsorbent Parameters

lobe diameter (mm)	1	external area (m²/m³)	1180
lobe height (mm)	5	pellet porosity[a]	0.5
particle density (kg.m⁻³)	1143	tortuosity[b]	4
pore diameter (10^{-10} m)	6	Si/Al	47−70

[a] The pellet porosity is an estimated parameter. The influence of this parameter will be discussed later. [b] Experimental tortuosity generally ranges between 2 and 6 (7). We have chosen a value of 4.
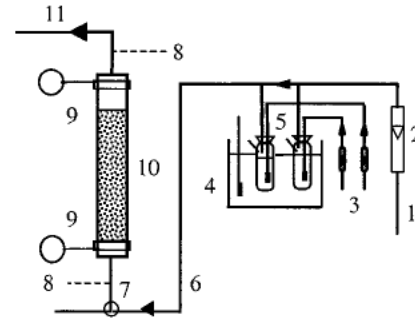

FIGURE 1. Adsorption column. 1, air inlet; 2 and 3, flowmeter; 4, thermostat tank; 5, bubblers; 6, inlet gas; 7, three-valve outlet; 8, gas-sample outlet; 9, pressure gauge; 10, adsorption bed; 11, outlet gas.

TABLE 2. Experimental Conditions for Breakthrough Curves

T, temp (K)	293.15
D, fluid flow (m³ h⁻¹)	2
ϵ, bed porosity	0.4
humidity of inlet air (%)	0
H, bed height (m)	0.20
u, superficial velocity (m s⁻¹)	0.29
ρ_l, bed density (kg m⁻³)	700

gives the adsorbent hydrophobic characteristics. The pellets are tri-lobe particles, composed of microporous crystals of zeolite (20−40 μm) included in a binder (16% mass). The main characteristics of the adsorbent are given in Table 1.

Adsorbate. Four different VOCs were used: n-heptane (99%), n-octane (99%), acetone (99.9%), and methyl ethyl ketone (MEK) (99.5%). They were chosen as they are present in industrial solvents. Moreover, these compounds have different volatilities and polarities.

Adsorption Equilibrium Experiments. A batch reactor (volume about 1 L) was used to obtain adsorption isotherms. It was placed in a thermostated tank. The zeolite sample was kept at 150 °C for 48 h and then cooled in a dry atmosphere before the experiments. The mass of zeolite used ranged from 0.5 to 4 g. The air/VOC mixture was obtained by injection of a known mass of VOC in liquid form by means of a syringe through a septum. The zeolites were put into contact with the air/VOC mixture by rotating an angled tube when all the liquid had evaporated. The gas was homogenized by a magnetic mixer. Gas samples were taken with an airtight syringe at equilibrium (1 h) and injected into an HP 5890 series II gas chromatograph equipped with a flame ionization detector (FID). The time to reach equilibrium was determined after several experiments at the same conditions for different times. The amount adsorbed after 1 h was the same as for 3 and 5 h.

Experimental Breakthrough Curve. The experimental setup used was the same as in Brosillon et al.'s previous work (19) (Figure 1); the experimental conditions are summarized in Table 2. Pellets of zeolite were packed in a fixed bed. The air/VOC mixture obtained using a bubbler was

TABLE 3. Constants for Langmuir Isotherm Equation

	b	q_{max} (mol/kg)
acetone	165	1.28
MEK	269	1.2
n-heptane	250	0.73
n-octane	253	0.56

diluted with dry air and injected at the bottom of the column. Samples were taken at the inlet and outlet of the column.

Parametric Value. The k_f coefficient was evaluated by means of Petrovic and Thodos's expression (20):

$$k_f = Re^{0.64} Sc^{0.33} \tag{10}$$

$$3 < Re < 900$$

The experiments work gave Re and Sc equal to 39 and 1.42, respectively. Axial dispersion was evaluated from the Wen and Fan (21) expression:

$$\frac{1}{Pe} = \frac{0.3}{ReSc} + \frac{1}{Pe_\infty}\frac{1}{\left(1 + \frac{3.2}{ReSc}\right)} \tag{11}$$

where

$$Pe_\infty = 2 \quad 0.4 < \epsilon < 0.5$$

With eq 11, we found Pe equal to 2.3. Note that the Schmidt and Peclet numbers are given for acetone and that the values for the other components are very close. The calculated value demonstrates that it is a reasonable approximation to neglect axial dispersion. This approximation was confirmed by calculating $(D_{col}/2R_p) = 26$ and $(L/2R_p) = 100$ (22). Radial dispersion could be neglected in the same way. Equivalent diameter was obtained using the characteristic length (23) given as $L' = V_p/S_p$ and $R_p = 6L'$. The R_p value found is equal to 2×10^{-3} m. Diffusivity coefficients (D_m) were obtained by means of the Chapman Enskog correlation (24).

Results and Discussion

Initially, the equilibrium constants of the Langmuir equation were determined (Table 3).

Convergence of the Model. For the prediction of the breakthrough curves, the system formed by eqs 1−5 was solved. The column was divided into N equal increments ($\Delta z = 1/N$), and the convergence was studied by increasing the value of N. Calculated breakthrough curves converge when N is greater than 25. We used N equal to 30 to ensure that there was no error due to numerical resolution of the system. The main advantage of the approach developed in this work is that the parameters appearing in the model can easily be estimated from correlations or determined from simple batch experiments. In addition, this model does not require much computing time.

Effect of Mass-Transfer Coefficients on Calculated Breakthrough Curves. To improve the model and to study the parametrical effects on the breakthrough curves, a parameter sensitivity analysis was performed. The sensitivity of the two mass-transfer coefficients k_f and k_p are shown in Figures 2 and 3. Referring to Figure 2, we see that the sensitivity of the external mass transfer is low. The importance of the effect of k_p variations is shown in Figure 3. In this case, the sensitivity of the k_p parameter is high, so it can be deduced that the overall mass transfer is controlled by internal mass transfer. Results obtained in our work corroborate the known information about gaseous adsorption: the external mass-transfer resistance is less important than the internal mass-transfer resistance. Our results are consistent with this.
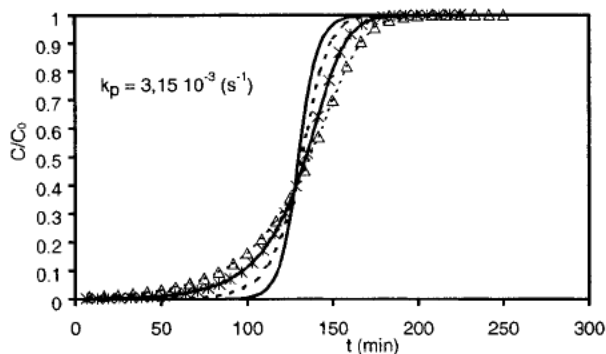

FIGURE 2. Influence of k_f parameter on predicted breakthrough curve. (−) k_f, (− −) $k_f/3$, (*) $k_f/6$, (△) $k_f/9$.
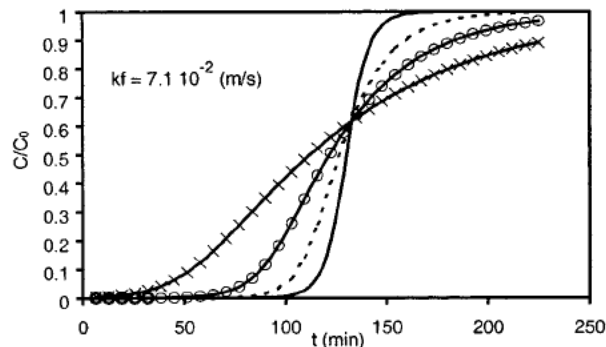

FIGURE 3. Influence of k_p parameter on predicted breakthrough curve. (−) k_p, (− −) $k_p/3$, (○) $k_p/6$, (×) $k_p/12$.
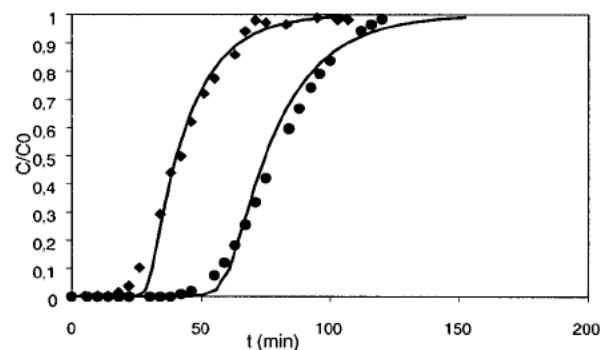

FIGURE 4. Experimental and predicted breakthrough curves for acetone and MEK. (◆) MEK, (●) acetone, (−) model.

Comparison between Experimental and Numerical Results. The K and k_p values are summarized in Table 4 for the different experimental runs. Examples of the reasonably good agreement between the model and the experimental breakthrough curves are shown in Figures 4 and 5 for the four components.

The k_p values range between 1.5×10^{-4} and 12.3×10^{-4} (s^{-1}). These are different from results published for light hydrocarbons on activated carbon (12), which give values of about 7×10^{-3} and 0.65 s^{-1}. Resistance in zeolite seems to be higher than in carbon. For adsorption of phenol and *p*-chlorophenol on activated carbon in the liquid phase (14), the k_p values range between 1.6×10^{-4} and 5.2×10^{-4} s^{-1}. These results show that the amplitude of internal mass-transfer resistance is comparable for the gas/zeolite and liquid/activated carbon systems, even if the internal transport phenomena are different.

Figure 6 shows the values of the internal mass-transfer coefficient as a function of the equilibrium constant (K) for acetone, MEK, *n*-heptane, and *n*-octane. For the four

TABLE 4. Experimental and Calculated Mass-Transfer Parameters for VOCs Adsorption

runs	C_e (mol m^{-3})	K	k_p (s^{-1})	D_e (cm^2 s^{-1})	D_k (cm^2 s^{-1})	D_k/D_e	D_s (cm^2 s^{-1})
acetone 1	0.20	9 077	12.3 × 10^{-4}	0.015	1.32 × 10^{-3}	0.07	5.4 × 10^{-6}
acetone 2	0.23	8 687	13.3 × 10^{-4}	0.015	1.32 × 10^{-3}	0.07	5.8 × 10^{-6}
acetone 3	0.13	12 488	9.01 × 10^{-4}	0.015	1.32 × 10^{-3}	0.07	8.3 × 10^{-6}
acetone 4	0.006	62 076	2.42 × 10^{-4}	0.020	1.32 × 10^{-3}	0.05	1 × 10^{-6}
acetone 5	0.06	6 528	5.74 × 10^{-4}	0.011	1.18 × 10^{-3}	0.10	4.9 × 10^{-6}
MEK 1	0.20	7 018	11.3 × 10^{-4}	0.010	1.18 × 10^{-3}	0.09	2.9 × 10^{-6}
MEK 2	0.11	11 721	6.63 × 10^{-4}	0.020	1.18 × 10^{-3}	0.05	3 × 10^{-6}
MEK 3	0.06	22 057	6.75 × 10^{-4}	0.017	1.18 × 10^{-3}	0.06	1.9 × 10^{-6}
MEK 4	0.04	29 287	4.34 × 10^{-4}	0.04	1.00 × 10^{-3}	0.02	1.2 × 10^{-6}
heptane 1	0.006	109 382	2.71 × 10^{-4}	0.016	1.00 × 10^{-3}	0.05	6.6 × 10^{-7}
heptane 2	0.01	78 423	1.50 × 10^{-4}	0.010	1.00 × 10^{-3}	0.08	5.9 × 10^{-6}
heptane 3	0.14	5 597	13.4 × 10^{-4}	0.010	1.00 × 10^{-3}	0.08	2.6 × 10^{-6}
heptane 4	0.07	11 929	6.08 × 10^{-4}	0.010	9 × 10^{-4}	0.07	2.7 × 10^{-6}
octane 1	0.04	12 291	6.27 × 10^{-4}	0.010	9 × 10^{-4}	0.07	1.8 × 10^{-6}
octane 2	0.03	19 250	4.20 × 10^{-4}	0.015	9 × 10^{-4}	0.05	8.8 × 10^{-7}
octane 3	0.01	56 145	1.99 × 10^{-4}	0.015	9 × 10^{-4}	0.05	8.8 × 10^{-7}
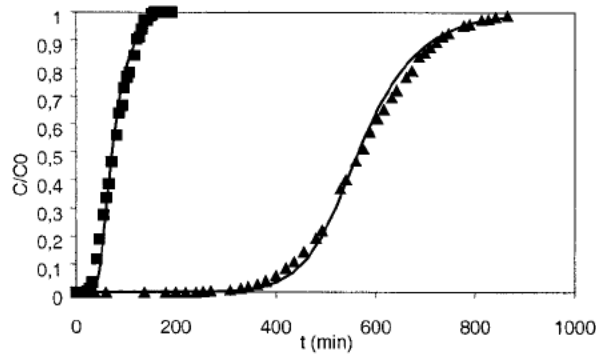
FIGURE 5. Experimental and predicted breakthrough curves for *n*-heptane and *n*-octane. (▲) heptane, (■) octane, (—) model.
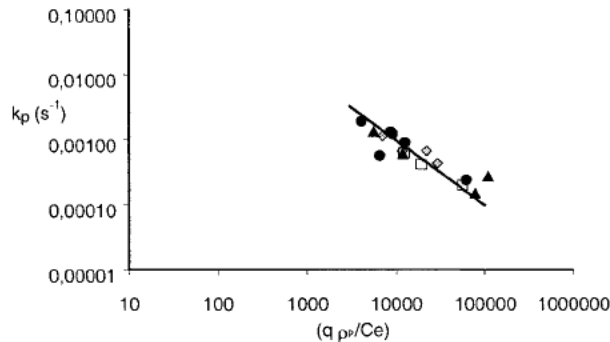
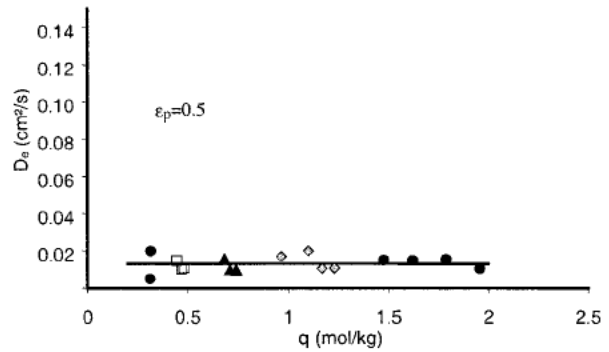**FIGURE 6.** Variation of k_p parameter with equilibrium constant. (●) acetone, (◆) MEK, (▲) heptane, (□) octane.

FIGURE 7. Variation of effective diffusivity with amount adsorbed. (●) acetone, (◆) MEK, (▲) heptane, (□) octane, (—) $D_{e,av}$.

components, the k_p values show a monotonically decreasing trend as the equilibrium constant increases. Malek and Farooq (*12*) also found this with linear hydrocarbons. This work shows that the behavior is the same for two different classes of products: linear hydrocarbon and ketone.

Estimation of Diffusivity. As shown above, external mass-transfer resistance can be neglected, so eq 7 becomes

$$\frac{1}{k_p} = \frac{R_p^2}{15\epsilon_p D_e}K \qquad (12)$$

The effective diffusivity values calculated with this relationship are presented in Table 7. These results are slightly higher than those found in the literature (*8, 12, 24*). This difference can be explained by the fact that the effective diffusivity is expressed on a gas-phase concentration basis. If the comparison is made on the D_e/K ratio, the published results become closer to our results (*17, 24*).

Relation between LDF Coefficient and Equilibrium Constant. The variation of effective diffusivity versus amount adsorbed is shown in Figure 7. We made the hypothesis that the internal porosity of the pellet (ϵ_p) was 0.5. A constant value was observed with increasing values of amount adsorbed, so it is consistent to calculate an average effective diffusivity ($D_{e,av}$) valid for the four different components. Equation 12 can be written as follows:

$$\frac{1}{k_p} = \frac{R_p^2}{15\epsilon_p D_{e,av}}K \qquad (13)$$

with $D_{e,av} = 0.013$ cm^2 s^{-1} determined from the slope of the solid line in Figure 7. In this way, an expression relating the LDF coefficient and equilibrium constant can be obtained. This same approach was followed by Malek and Farooq (*12*). Our results give an extension since they incorporate components from different chemical classes and polarities. This allows the prediction of breakthrough curves for other VOCs adsorbed onto zeolite to be predicted by means of eq 13. To know the influence of porosity of the adsorbent on mass transfer, we have calculated the effective diffusivity for each run with different porosity. On the basis of this calculation, we get an average effective diffusivity: 0.022, 0.016, and 0.013 cm^2 s^{-1} for porosities equal to 0.3, 0.4, and 0.5, respectively. These results show the importance of porosity of the adsorbent on the mass-transfer phenomenon. However, it is difficult to provide more detailed investigation about the influence of the structure of the commercial zeolite because of the complexity of the structure of this adsorbent (biporous, unknown tortuosity, different size of microcrystal). Hence, we have chosen a lumped model to describe the mass transfer in the adsorbent.

Surface Diffusivity. The calculation of the ratio D_k/D_e using the experimental values allows an estimation of the contribution of Knudsen diffusivity in the internal transport. These values are included in Table 4 and show that the Knudsen diffusivity has only a slight importance and that intraparticle transport is mainly concerned by surface diffusion. Indeed the mean pore radius of zeolite is very small, close to the molecule size, and involves transport of compounds in the adsorbate state. Surface diffusivity (D_s) was calculated by means of eq 9 with the assumption that surface tortuosity and pore tortuosity were the same and equal to 4 (*26*). The values are of the same order as the surface diffusivity obtained for linear hydrocarbon on activated carbon (*9*) and NaX zeolite (*27*).

Nomenclature

b	Langmuir constant
C	gas concentration (mol m^{-3})
C_s	gas concentration at the surface of the pellet (mol m^{-3})
C_e	gas concentration at equilibrium (mol m^{-3})
C_0	initial concentration (mol m^{-3})
D	fluid flow (m^3 h^{-1})
D_c	micropore diffusivity (m^2 s^{-1})
D_{col}	column diameter (m)
D_e	effective diffusivity (m^2 s^{-1})
$D_{e,av}$	average effective diffusivity (m^2 s^{-1})
D_k	Knudsen diffusivity (m^2 s^{-1})
D_m	molecular diffusivity (m^2 s^{-1})
D_p	porous diffusivity (m^2 s^{-1})
D_s	surface diffusivity (m^2 s^{-1})
H	height of bed (m)
K	equilibrium constant
k_f	interphase mass-transfer coefficient (m s^{-1})
k_p	intrapellet mass-transfer coefficient (s^{-1})
L'	characteristic length (m)
M	molecular weight (g mol^{-1})
N	number of increments
q	moles of adsorbate adsorbed per unit mass of adsorbent (mol kg^{-1})
q_{max}	maximum adsorbed phase concentration (mol kg^{-1})
q_s	concentration adsorbed on the surface of adsorbent (mol kg^{-1})
r_o	mean pore radius (m)
R	ideal gas constant (8.3145 J mol^{-1} K^{-1})
R_c	radius of microparticle (m)
R_p	equivalent radius of pellet (m)
S_p	external area (m^2 m^{-3})
S_p'	external area of one pellet (m^2)
t	time (s)
T	temperature (K)
u	superficial velocity (m s^{-1})
V_p	volume of a pellet (m^3)
z	axial coordinate in the column (m)
ϵ	porosity of bed
ϵ_p	porosity of particle
ρ_p	density of adsorbent (kg m^{-3})
ρ_l	bed density (kg/m^{-3})
$\tau_{p,s}$	tortuosity, pore, surface

Dimensionless Numbers

Re	Reynolds number
Sc	Schmidt number
Pe	Peclet number

Literature Cited

(1) Manero, M. H.; Jain, R. K.; Aurelle, Y.; Cabassud, C.; Roustan, M. *Environmental Technologies and Trends*; Shelton, S. P., Ed.; Springer: New York, 1996; pp 83−97.
(2) Fajula, F.; Plee, D.; Jansen, J. C.; Stöcker, M.; Karge, H. G.; Weitkamp, J. *Gas and Liquid Separations, Studies in Surface Science and Catalogs*; Elsevier: Amsterdam, 1994; p 633.
(3) Le Cloirec, P.; Dagois, G.; Martin, G. *Traitements avec Transfer Gaz-Solide: l'Adsorption, Odeurs et Désodorisation dans l'Environnement*; Lavoisier Tec & Doc: Paris, 1991.
(4) Cal, M. P.; Larson, S. M.; Rood, M. *J. Environ. Prog.* **1994**, *13*, 26−30.
(5) Tien, C. *Adsorption Calculations and Modelling*; Butterworth-Heinemann: Washington, 1994.
(6) Suzuki, M. *Adsorption Engineering*; Kodansha, Ed.; Elsevier: Amsterdam, 1990.
(7) Ruthven; D. *Principles of Adsorption and Adsorption Processes*; John Wiley and Sons: New York, 1984.
(8) Costa, E.; Callega, G.; Domingo, F. *AIChE J.* **1985**, *31* (6), 982.
(9) Huang, C. C.; Fair, J. R *AIChE J.* **1988**, *34* (11), 1861−1877.
(10) Delage, F.; Pré, P.; Le Cloirec, P. *Environ. Sci. Technol.* **2000**, *34* (22), 4816−4821.
(11) Chenu, M.; Bouzaza, A.; Wolbert, D.; Laplanche, A. *Environ. Technol.* **1998**, *19*, 1029−1038.
(12) Malek, A.; Farooq, S. *AIChE J.* **1997**, *43*, 761−776.
(13) Chandak, M. V.; Lin, Y. S. *Environ. Technol.* **1998**, *19*, 941−948.
(14) Moon, H.; Lee, W. K. *Chem. Eng. Sci.* **1986**, *41* (8), 1995−2004.
(15) Langmuir, I. *J. Am. Chem. Soc.* **1918**, *40*, 1361.
(16) Glueckauf, E. *Trans. Faraday Soc.* **1955**, *51*, 1540.
(17) Karger, J.; Ruthven, D. M. *Diffusion in Zeolites and Other Microporous Solids*; Wiley: New York, 1992.
(18) Meier, W. M.; Olson, D. H. *Atlas of Zeolite Structure Types*; Butterworth-Heinmann: Boston, 1992.
(19) Brosillon, S.; Manero, M. H.; Foussard, J. N. *Environ. Technol.* **2000**, *21*, 457−465.
(20) Petrovic, L. J.; Thodos, G. *Ind. Eng. Chem. Fundam.* **1968**, *7*, 274.
(21) Wen, C. Y.; Fan, L. T. *Models for Flows Systems and Chemical Reactors*; Marcel Dekker: New York, 1975.
(22) Raghavan, N. S.; Ruthven, D. M. *AIChE J.* **1983**, *29*, 922.
(23) Villermaux, J. *Génie de la Réaction Chimique;* Lavoisier Tec & Doc: Paris, 1993; Chapter 8, pp 297−346.
(24) Bird, R. B.; Stewart, W. E.; Lightfoot, E. N. *Transport Phenomena*; Wiley: New York, 1960.
(25) Haag, W. O.; Lago, R. M.; Weisz, P. B. *Discuss. Faraday Soc.* **1982**, *72*, 317.
(26) Post, M. F. M.; Van Amstel, J.; Kouwenhoven, H. W. *Proceedings of the 6th International Zeolite Conf*erence; Butterworth: Guildford, 1984; p 517.
(27) Satterfield, C. N. *Heterogeneous Catalysis in Practice*; McGraw-Hill: NewYork, 1980.
(28) Kärger, J.; Ruthven, D. M. *J. Chem. Soc. Faraday Trans.* **1981**, *I 77*, 1485.